Ocean Sci., 12, 937–951, 2016
www.ocean-sci.net/12/937/2016/
doi:10.5194/os-12-937-2016

Ocean Science Open Access EGU

Aragonite saturation states and pH in western Norwegian fjords: seasonal cycles and controlling factors, 2005–2009

Abdirahman M. Omar[1,2], **Ingunn Skjelvan**[1], **Svein Rune Erga**[3], **and Are Olsen**[2]

[1]Uni Research Climate, Bjerknes Centre for Climate Research, Bergen, Norway
[2]Geophysical Institute, University of Bergen, and Bjerknes Centre for Climate Research, Bergen, Norway
[3]Department of Biology, University of Bergen, Bergen, Norway

Correspondence to: Abdirahman M. Omar (abdir.Omar@uni.no)

Received: 26 February 2016 – Published in Ocean Sci. Discuss.: 17 March 2016
Revised: 29 June 2016 – Accepted: 30 June 2016 – Published: 26 July 2016

Abstract. The uptake of anthropogenic carbon dioxide (CO_2) by the ocean leads to a process known as ocean acidification (OA), which lowers the aragonite saturation state (Ω_{Ar}) and pH, and this is poorly documented in coastal environments including fjords due to lack of appropriate observations.

Here we use weekly underway data from the Voluntary Observing Ships (VOS) program covering the period 2005–2009 combined with data from research cruises to estimate Ω_{Ar} and pH values in several adjacent western Norwegian fjords, and to evaluate how seawater CO_2 chemistry drives their variations in response to physical and biological factors.

The OA parameters in the surface waters of the fjords are subject to strong seasonal and spatially coherent variations. These changes are governed by the seasonal changes in temperature, salinity, formation and decay of organic matter, and vertical mixing with deeper, carbon-rich coastal water. Annual mean pH and Ω_{Ar} values were 8.13 and 2.21, respectively. The former varies from minimum values (≈ 8.05) in late December – early January to maximum values of around 8.2 during early spring (March–April) as a consequence of the phytoplankton spring bloom, which reduces dissolved inorganic carbon (DIC). In the following months, pH decreases in response to warming. This thermodynamic decrease in pH is reinforced by the deepening of the mixed layer, which enables carbon-rich coastal water to reach the surface, and this trend continues until the low winter values of pH are reached again. Ω_{Ar}, on the other hand, reaches its seasonal maximum (>2.5) in mid- to late summer (July–September), when the spring bloom is over and pH is decreasing. The lowest Ω_{Ar} values (≈ 1.3–1.6) occur during winter (January–March), when both pH and sea surface temperature (SST) are low and DIC is its highest. Consequently, seasonal Ω_{Ar} variations align with those of SST and salinity normalized DIC (nDIC).

We demonstrate that underway measurements of fugacity of CO_2 in seawater (fCO_2) and SST from VOS lines combined with high frequency observations of the complete carbonate system at strategically placed fixed stations provide an approach to interpolate OA parameters over large areas in the fjords of western Norway.

1 Introduction

The continued emissions of carbon dioxide (CO_2) (Le Quéré et al., 2015) are of global concern, not only because they are the main driver of anthropogenic global warming, but also because of the changes in the ocean chemistry they cause (Ciais et al., 2013). The increase in the atmospheric CO_2 concentration drives a net ocean CO_2 uptake, which leads to higher proton (H^+) concentration, i.e. lower pH, lower concentration of carbonate ion (CO_3^{2-}), and lower saturation state (Ω) for calcium carbonate in seawater. This process is known as ocean acidification (OA) (e.g. Royal Society, 2005), and it has direct and indirect effects on biological activity in the ocean (e.g. Gattuso and Hansson, 2011) including reported inhibition of biogenic calcification by marine organisms, which precipitate 0.5–2.0 Gt of carbon as calcium carbonate ($CaCO_3$) in the global ocean every year (Bach, 2015).

For the open ocean, the rate of OA has been relatively well documented and understood during the last decade. Observations from time series stations and voluntary observing ships in different oceanic regions consistently show systematic changes in surface ocean chemistry that result from OA. Specifically, long-term negative trends of pH and saturation state for aragonite (Ω_{Ar}) have been observed (e.g. Lauvset et al., 2015; Bates et al., 2014).

For coastal regions observed rates of pH change largely differ from those expected from oceanic CO_2 uptake alone, as variations in other biogeochemical processes, related for example to changes in nutrient loading and eutrophication, are important as well (Clargo et al. 2015; Provoost et al., 2010; Wootton et al., 2008).

The Norwegian west coast (Fig. 1) is dominated by fjords, narrow and deep estuaries, carved by glacial processes, with a sill in the mouth where they connect to the coastal North Sea. Apart from being important recreation areas and marine pathways, these fjords are important ecosystems and their physics, marine life, and associated environmental pressures have been relatively well studied (e.g. Matthews and Sands, 1973; Erga and Heimdal, 1984; Asplin et al., 2013; Brattegard et al., 2011; Stigebrandt, 2012; and references therein).

However, only a few studies on the carbon cycle of Norwegian fjords exist and these are only from the high Arctic at Svalbard (Fransson et al., 2014; Omar et al., 2005). Generally, in the Northern Hemisphere, high latitude coastal regions are thought to be sinks for atmospheric CO_2, while low-latitude regions are thought to be CO_2 sources (Borges et al., 2005; Cai et al., 2006; Chavez et al., 2007; Chen and Borges, 2009). The few existing studies of Norwegian fjords confirm the above picture; i.e. they act as an annual net sink for atmospheric CO_2 (Fransson et al., 2014; Omar et al., 2005).

The carbon cycle of the northern North Sea, to which the western Norwegian fjords are connected, has been well studied (Thomas et al., 2004, 2005, 2007, 2009; Bozec et al., 2005, 2006; Omar et al., 2010). However, observation-based OA estimates are still scarce. Recently, Clargo et al. (2015) observed a rapid pH decrease in the North Sea, but after accounting for biological processes, they estimated an ocean acidification rate consistent with concurrent atmospheric and open-ocean CO_2 increases over the period they studied, 2001–2011.

Filling the knowledge gap on OA (and generally the carbon cycle) in western Norwegian fjords is important because these areas are spawning grounds for different fish species (Salvanes and Noreide, 1993; Johannessen et al., 2014), production sites for pelagic calcifiers (Berge, 1962; Erga and Heimdal, 1984; Frette et al., 2004), the home for some coral reefs (e.g. Fosså et al., 2002), and significant food sources due to the aquaculture industry that operates there. Observations of the carbon cycle dynamics in the fjord system will not only further our understanding and ability for prediction, but also serve as benchmarks against which future changes are compared.

In this study, we present first estimates of OA parameters in surface waters of several adjacent western Norwegian fjords (Fig. 1), based mainly on weekly underway data from the Voluntary Observing Ships (VOS) program covering the period 2005–2009. We combine the underway data with available station data from research cruises to facilitate a complete description of the seawater CO_2 chemistry in accordance with the recommendations of OA core principles by McLaughlin et al. (2015). We focus on analyses of Ω_{Ar} and pH values and evaluate their variations in response to the physical and biological factors: summer warming and stratification, spring phytoplankton bloom, and deep mixing during fall and winter. First we present the mean distribution across the different fjords (Korsfjord–Langenuen–Hardangerfjord) to understand the spatiotemporal patterns, then we collapse all data into a monthly time series to analyse the seasonal controls and resolve any interannual or multiyear temporal patterns.

1.1 The study area

The study area covers, from north to south, the interconnected Raunefjord (centred around 60.27° N, 5.17° E), the Korsfjord (centred around 60.17° N, 5.21° E), Langenuen, and southern parts of the Hardangerfjord, which are all situated along the western coast of mainland Norway (Fig. 1). The area stretches over some 60 km, but the main focus here will be on the area from the Korsfjord to the Hardangerfjord from which the vast majority of the data have been acquired.

The bathymetry and hydrographic conditions of the fjords have been described elsewhere (Helle, 1978; Mathew and Sands, 1973; Bakke and Sands, 1977; Erga and Heimdal, 1984; Asplin et al., 2014). In the following only a brief account, based on the above studies, is given.

The Korsfjord is 690 m deep in its main basin and situated about 25 km south of the Norway's second largest city, Bergen. To the west, Korsfjord is relatively well connected to the coastal North Sea through a 250 m deep sill at Marsteinen. To the north it connects with the Raunefjord through the 100 m deep strait Lerøysundet – between the islands Sotra and Lerøy. At the eastern end the fjord branches into the smaller and shallower fjords Lysefjord and Fanafjord, and to the southwest it connects with the coastal North Sea through the Selbjørnsfjord, which has a sill depth of 180 m at Selbjørn. To the south it connects to the Hardangerfjord through the 25 km long and 300 m deep strait Langenuen.

The Hardangerfjord is a 179 km long fjord ranking as the fourth longest fjord in the world. It stretches from the coastal open ocean in the southwest to the mountainous interior of Norway. Our study includes the southern parts of the fjord. This is bounded by the larger islands Stord and Tysnesøya in the north, the Haugaland peninsula in the south, and the

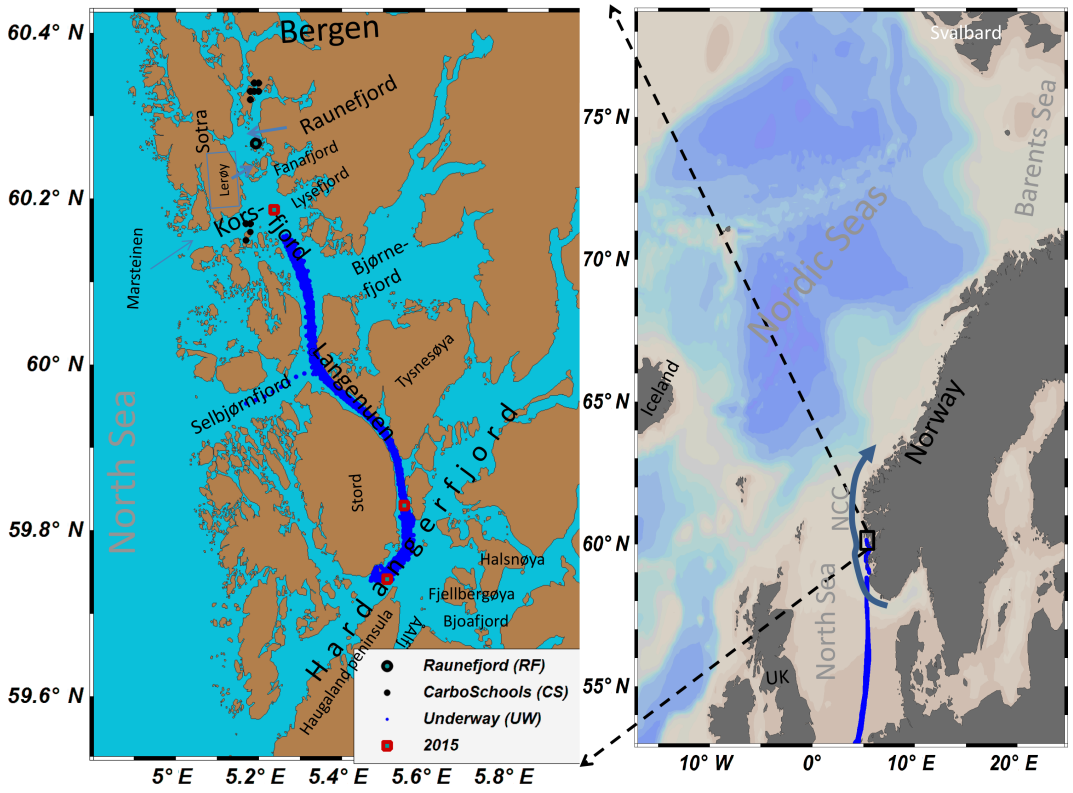

Figure 1. An overview map of western Norway with a detailed map of the study area showing the positions from where cruise and underway data have been acquired. The thick arrow on the right panel indicates the approximate position of the Norwegian Coastal Current (NCC).

smaller islands Fjellbergøya and Halsnøya on the southeast side. This part of the fjord is over 300 m deep in its basin (around 59.76° N, 5.55° E) and connects with the smaller fjords Ålfjord and Bjoafjord in the south.

In the fjord system, run-off from land mixes with salty water originating from the northward flowing Norwegian Coastal Current (NCC) to produce a typically salinity stratified water column with a complex circulation, forced both by external and internal factors. In particular, the coastal winds have a profound influence on the water circulation in western Norwegian fjords producing episodic renewal of the deep water that follows periods of prolonged northerly winds (Svendsen, 1981; Erga and Heimdal, 1984).

Besides wind forcing, the hydrography of the fjords is also influenced by winter cooling, summer warming, and run-off. The fjords also receive freshwater through the NCC, which carries water originating from the Baltic Sea and rivers in the southern North Sea (Skagseth et al., 2011 and references therein). On seasonal timescales, salinity drives stratification during spring–summer and the water column is more homogenous during winter. Additionally, Asplin et al. (2014) reported regular episodes of water exchange between Hardangerfjord and the NCC that homogenized the upper 50 m of the fjord by mixing with coastal water. During these events the water temperature inside the Hardangerfjord regularly becomes identical with that of the adjacent coastal North Sea (Asplin et al., 2014).

Water exchange with the NCC is important for the fjord ecosystems as it supplies nutrients and oxygen to the area (Aure and Stigebrandt, 1989). In response, primary production is enhanced in the fjords, which support rich and diverse marine life (Erga and Heimdal, 1984; Erga, 1989; Salvanes and Noreide, 1993).

Erga and Heimdal (1984) studied the dynamics of the spring bloom in the Korsfjord and estimated a total primary production of 74 g C m^{-2} during the period February–June. Further, they reported light regime and water column stability to be dominant controls of the onset of the bloom. They also pointed out that changes in the alongshore wind component are important for the bloom dynamics, with persistent northerly winds inducing upwelling of nutrient-rich coastal water that promotes blooming, whereas the opposite situation occurs from persistent southerly winds. During calm periods strong stratification develops, which can ultimately lead to nutrient exhaustion in the upper water column.

The study area, with its adjacent waters, is ecologically and economically important because it covers spawning grounds for a number of different fish species (Lie et al., 1978; Johannessen et al., 2014). Additionally, the largest concentration of coral reefs in western Norway is found in

the Langenuen strait (Fosså, 2015). The fjord system also contributes to the important aquaculture production that, with its annual fish production of >700 tonnes, ranks Norway within tenth place worldwide. About one-fifth of this is produced in the Hordaland County where the fjord system studied here is situated (http://www.diercke.com).

2 Data and methods

2.1 Weekly underway VOS data

Weekly underway measurements of fugacity of CO_2 in seawater (fCO_2) and sea surface temperature (SST) were obtained aboard the containership MS *Trans Carrier* (operated by Seatrans AS, Norway, www.seatrans.no). During the study period, the ship sailed from Bergen to ports in southwestern Norway on a weekly basis. It passed through several fjords including the Korsfjord and the Hardangerfjord (Fig. 1), then crossed the North Sea mostly along a transect roughly at 5° E longitude to Amsterdam, the Netherlands, and then back on the same route (Omar et al., 2010). The measurement method used aboard MS *Trans Carrier* was described in Omar et al. 2010). Briefly, the instrument uses a non-dispersive infrared CO_2 / H_2O gas analyser (LI-COR 6262) to determine the CO_2 concentration in a headspace air in equilibrium with a continuous stream of seawater. One analysis was done every 3 min and the instrument was calibrated roughly every 6 h with three reference gases, which are traceable to reference standards provided by National Oceanic and Atmospheric Administration – Earth System Research Laboratory (NOAA/ESRL). The instrument automatically shut off when the ship approached ports in Bergen (20–30 km from port ≈ 60.2° N) and Amsterdam, in order to protect the inlet filter from potentially polluted seawater. Between February and December 2006 the VOS line was serviced by a sister ship, MS *Norcliff*, which was equipped with the same measurement system during that period. The VOS line was in operation in the period September 2005 to September 2009. Data acquired between 59.74–60.16° N and 5.17–5.58° E (the Korsfjord, Langenuen, and southern parts of the Hardangerfjord) are used for the current analyses. This data set will be referred to as the UW (e.g. UW fCO_2 and UW SST), which stands for underway. The UW data from the years 2005, 2006, and 2007 are available from the SOCAT database (Bakker et al., 2014; http://www.socat.info/), the 2008 and 2009 UW data have been submitted for the SOCAT version 4 release.

2.2 Cruise and fixed station data

We augment the VOS data with station data acquired during scientific cruises in the study area in the period 2007–2010 and in 2015, and during regular visits (1–4 times per month) to a fixed station in the Raunefjord in 2007 and 2008. Table 1 summarizes details of these three data sets, which will be referred to as the CS, 2015, and RF data sets.

Five of the cruises were conducted in the Korsfjord and the Raunefjord (Fig. 1, Table 1) onboard RV *Hans Brattstrøm* as part of the EU FP7 educational project CarboSchools (CS) in 2007–2010. The CS data set covers mainly the spring and summer seasons reflecting the somewhat opportunistic nature of the sampling campaign. The 2015 cruise took place during fall (24 September) as part of the Ocean Acidification project funded by the Norwegian Environment Agency, and measurements were taken at three stations in Korsfjord, Langenuen, and southern Hardangerfjord (Fig. 1, red squares).

During each of the above cruises water samples were collected for analyses of parameters including dissolved inorganic carbon (DIC), total alkalinity (TA), salinity and temperature at 1–2 stations. The DIC concentrations were determined by the coulometric method (e.g. Johnson et al., 1993) with a precision of $\pm 1.2\,\mu mol\,kg^{-1}$. TA was measured by potentiometric titration with strong acid (HCl), and a precision of $\pm 4.8\,\mu mol\,kg^{-1}$. Accuracy was checked by using certified reference material supplied by A. Dickson at Scripps Institution of Oceanography. Once all samples have been corrected with respect to offsets determined from the CRM measurements, the DIC and TA measurements were accurate to within 1.4 times respective measurement precision (above). Only surface data (depth$<=4$ m) from within the geographical rectangle 59.74–60.34° N and 5.17–5.55° E were used in the current study.

The Department of Biology, University of Bergen, has acquired data for conductivity, temperature, and depth (CTD) from a fixed station in Raunefjord (RF) during 27 days in 2007 and 35 days in 2008 as part of a monitoring program close to the marine biological field station at Espegrend. These data contained temperature and salinity profiles with 1 m resolution. Averages of the uppermost 5 m have been used in this study and will be referred to as the RF data set.

2.3 In situ pH sensor data

In January 2012 we carried out an evaluation of two pH sensors of the type Submersible Autonomous Moored Instruments (SAMI_pH, second generation) at the marine biological field station at the eastern shore of the Raunefjord. The sensors were suspended from a wooden frame attached to the floating docks around a raft house in the fjord – some hundred metres from land. The instruments were submersed at about 1 m depth in the fjord and were left for 50 h starting 24 January 2012 10:00 GMT, recording one measurement each hour. A full description of the measurement method for these instruments is found at http://www.sunburstsensors.com/. In addition to pH, these instruments also recorded the seawater temperature and they have measurement precision and accuracy of <0.001 and ± 0.003 pH units, respectively. During the test, salinity was also recorded using a Seaguard Recording Current Meter (RCM) from Aanderaa Data Instru-

Table 1. Details of the CarboSchools (CS) and Raunefjord (RF) cruise data sets. The plus signs denote the parameters for which sampling/measurement were carried out. For the RF data set, each data point represents the average of five measurements acquired in the upper 5 m.

Data set; area	Date (mm/dd/yyyy)	Long (E)	Lat (N)	Depth (m)	DIC	TA	SST	SSS	Reference/ originator
CarboSchools (CS); Korsfjord/Raunefjord	04/13/2007	5.19	60.34	1	+	+	+	+	I. Skjelvan
	04/13/2007	5.18	60.17	1	+	+	+	+	
	04/25/2007	5.19	60.34	1	+	+	+	+	
	04/25/2007	5.17	60.17	1	+	+	+	+	
	09/04/2008	5.18	60.33	1	+	+	+	+	
	03/12/2009	5.17	60.15	1	+	+	+	+	
	03/12/2009	5.18	60.32	1	+	+	+	+	
	03/12/2009	5.17	60.17	1	+	+	+	+	
	03/12/2009	5.18	60.33	1	+	+	+	+	
	08/25/2009	5.17	60.17	1	+	+	+	+	
	08/24/2009	5.18	60.16	1	+	+	+	+	
	08/24/2009	5.18	60.16	1	+	+	+	+	
	08/24/2009	5.19	60.34	1	+	+	+	+	
	08/25/2009	5.19	60.34	1	+	+	+	+	
	08/25/2009	5.2	60.34	1	+	+	+	+	
	08/25/2009	5.19	60.33	1	+	+	+	+	
	08/27/2009	5.19	60.33	1	+	+	+	+	
	08/27/2009	5.19	60.33	1	+	+	+	+	
	08/27/2009	5.18	60.17	1	+	+	+	+	
	08/27/2009	5.18	60.17	1	+	+	+	+	
	08/27/2009	5.18	60.17	1	+	+	+	+	
	08/27/2009	5.2	60.33	1	+	+	+	+	
	09/08/2010	5.2	60.33	1	+	+	+	+	
2015; Korsfjord	09/29/2015			5	+	+	+	+	I. Skjelvan/A. Omar
2015; Langenuen	09/29/2015			5	+	+	+	+	I. Skjelvan/A. Omar
2015; Hardangerfjord	09/29/2015			5	+	+	+	+	I. Skjelvan/A. Omar
RF; Raunefjord	01/03/2007			1–5			+	+	S. R. Erga/J. Egge
	01/23/2007			1–5			+	+	
	02/13/2007			1–5			+	+	
	02/27/2007			1–5			+	+	
	03/07/2007			1–5			+	+	
	03/13/2007			1–5			+	+	
	03/27/2007			1–5			+	+	
	04/10/2007			1–5			+	+	
	04/17/2007			1–5			+	+	
	04/23/2007			1–5			+	+	
	05/08/2007			1–5			+	+	
	05/19/2007			1–5			+	+	
	06/05/2007			1–5			+	+	
	06/12/2007			1–5			+	+	
	06/19/2007			1–5			+	+	
	08/31/2007			1–5			+	+	
	09/04/2007			1–5			+	+	
	09/11/2007			1–5			+	+	
	09/18/2007			1–5			+	+	
	09/26/2007			1–5			+	+	
	10/02/2007			1–5			+	+	
	10/09/2007			1–5			+	+	
	10/18/2007			1–5			+	+	
	10/31/2007			1–5			+	+	
	11/27/2007			1–5			+	+	
	12/11/2007			1–5			+	+	

Table 1. Continued.

Data set; area	Date (mm/dd/yyyy)	Long (E)	Lat (N)	Depth (m)	DIC	TA	SST	SSS	Reference/ originator
	01/02/2008			1–5			+	+	
	02/05/2008			1–5			+	+	
	02/21/2008			1–5			+	+	
	03/05/2008			1–5			+	+	
	03/11/2008			1–5			+	+	
	03/25/2008			1–5			+	+	
	03/31/2008			1–5			+	+	
	04/08/2008			1–5			+	+	
	04/22/2008			1–5			+	+	
	04/29/2008			1–5			+	+	
	05/06/2008			1–5			+	+	
	05/13/2008			1–5			+	+	
	05/20/2008			1–5			+	+	
	05/27/2008			1–5			+	+	
	06/04/2008			1–5			+	+	
	06/11/2008			1–5			+	+	
	06/17/2008			1–5			+	+	
	06/24/2008			1–5			+	+	
	07/01/2008			1–5			+	+	
	07/08/2008			1–5			+	+	
	07/16/2008			1–5			+	+	
	08/12/2008			1–5			+	+	
	08/19/2008			1–5			+	+	
	08/26/2008			1–5			+	+	
	09/02/2008			1–5			+	+	
	09/09/2008			1–5			+	+	
	09/16/2008			1–5			+	+	
	09/23/2008			1–5			+	+	
	09/30/2008			1–5			+	+	
	10/07/2008			1–5			+	+	
	10/14/2008			1–5			+	+	
	10/21/2008			1–5			+	+	
	11/04/2008			1–5			+	+	
	11/20/2008			1–5			+	+	
	12/19/2008			1–5			+	+	

ments. These sensor data were used to assess the uncertainty in our pH values estimated as described in Sect. 3.1.

2.4 Methods

2.4.1 Complete seawater CO_2 chemistry from SST and fCO_2

We obtained a complete description of the seawater CO_2 chemistry from the UW SST and UW fCO_2 data collected onboard MS *Trans Carrier* through a 3-step procedure as described below. This is similar to the procedure described in Nondal et al. (2009) with the main modification being that in the current study, sea surface salinity (SSS) was determined from an empirical relationship with SST.

First, the RF data set has been used to determine the regional SSS vs. SST relationship. The RF data were chosen for this purpose because it covered all seasons well, both in 2007 and 2008. The identified regional SSS–SST relationship allowed us to estimate a SSS value for each UW SST observation from MS *Trans Carrier*. This step was necessary because the total number of measured SSS values were less than 150 data points, while the available underway SST and fCO_2 data were much more numerous (> 9900 data points), covering most of the study area during the years 2005–2009. The remaining SST and SSS data (CS, and from sensors) were used for evaluation to verify that SST–SSS relationship is valid for the whole study area (Sect. 3.1). Salinity values estimated from SST will be denoted as SSS(sst).

Second, we determined TA from SSS(sst) and SST using an algorithm we identified for the region using the CS data set. This allows us to estimate a corresponding alkalinity value for each UW fCO_2 observation obtained from MS

Trans Carrier. Alkalinity values estimated from measured SSS and SST data will be denoted as TA(sss), whereas TA values estimated from SSS(sst) and SST values will be denoted as TA(sst).

The UW fCO_2 together with TA (sst), UW SST, and SSS(sst) were then used to characterize the full seawater CO_2 chemistry using CO2SYS (Lewis and Wallace, 1998; van Heuven et al., 2011), with K1 and K2 constants from Lueker et al. (2000). The concentration of silicate and phosphate has been put to zero during the calculations, and the errors introduced by this simplification were negligible compared to the uncertainties from other sources (to be described in Sect. 3.1). The CO2SYS calculation also gives DIC, pH, Ω_{Ar}, and all other seawater CO_2 chemistry variables. The data estimated using this three stage procedure will be denoted pH(sst) and Ω_{Ar}(sst) and are the main focus of this study.

pH and Ω_{Ar} values based on TA(sss) and fCO_2 will be denoted as pH(sss) and Ω_{Ar}(sss), whereas values that are either measured or computed from measured TA and DIC will be denoted as simply pH and Ω_{Ar}. nDIC denotes the DIC values normalized to constant salinity (the mean value) according to Friis et al. (2003) with freshwater endmember DIC concentration of $1039\,\mu mol\,kg^{-1}$ inferred from the cruise data. An overview of the symbols used for estimated and derived quantities used in this study is given in Table 2.

3 Results and discussion

3.1 Correlations and validations

In this section we present the regression equations identified in this study in addition to validating the various estimation procedures used by comparing the estimated values with those measured/computed. The results of these comparisons are summarized in Table 3. For each comparison, the coefficient of determination (R^2) and the significance level (p-value) are used as metrics for the goodness of the correlation while the associated root mean square error (RMSE) is benchmarked against the maximum target uncertainties developed by the Global Ocean Acidification Observing Network (GOA-ON) and the California Current Acidification Network (C-CAN) of ± 0.2 for Ω_{Ar} (McLaughlin et al., 2015), which corresponds to maximum uncertainties of ± 0.02, ± 1.25, or ± 1.8 in pH, SST, or SSS, respectively.

The regional SST-SSS relationship obtained from the RF data set is given by Eq. (1) and is depicted in Fig. 2a (filled symbols). Despite a clear covariation between SST and SSS, there is a lot of scatter in the data and the statistics of the regression equation is not particularly strong (Eq. 1). The observed correlation most probably arises from the annual cycles; during summer the study area embodies warm water diluted by run-off, whereas during winter the surface water is colder and saltier due to little or no run-off. The magnitude of these annual variations varies with time and space and this is reflected by the high degree of scatter in the relationship. Consequently, the identified regression model is able to explain only 27 % of the salinity variations. Nonetheless, the independent station and sensor data (dots, squares, and stars), which have been acquired from the whole study area in different seasons, falls into a pattern around the relationship described by Eq. (1) with a RMSE of 0.81. Thus, we assume that Eq. (1) is able to estimate the seasonal SSS variations across the whole study region. To verify this we have compared the monthly averages of RF_SSS data with values obtained using Eq. (1) and monthly RF_SST. As shown in the last row of Table 3, the estimated values were significantly correlated with the monthly RF_SSS ($R^2 = 0.65$ and $p = 0.002$) and the resulting RMSE of 0.3 was lower than the benchmark values of ± 1.8.

$$\begin{aligned} &SSS = -0.142SST + 32.09, \text{for } \; SSS > 29 \\ &R^2 = 0.27; n = 61; RMSE = 1.2. \end{aligned} \quad (1)$$

As further verification that the RF SST data set is spatially representative, we compared it with the chronologically co-located UW SST that have been acquired onboard MS *Trans Carrier* across the whole study area. The two data sets were found to be almost identical (Fig. 2b; 3rd row Table 3).

The relationship between TA, SSS, and SST obtained from the CS and 2015 data sets is given by Eq. 2 according to

$$\begin{aligned} &TA = 32.09SSS - 4.39SST + 1210 \\ &R^2 = 0.90; n = 23; \text{RMSE} = 13.0\,\mu molkg^{-1}. \end{aligned} \quad (2)$$

Alkalinity is a semi-conservative variable and is normally modelled as a linear function of salinity (e.g. Millero et al., 1998; Bellerby et al., 2005; Nondal et al, 2009). However, using a multi-parameter linear regression with SST and SSS as independent parameters improved the regression statistics considerably ($R^2 = 0.90$; $n = 23$; $\text{RMSE} = 13.0\,\mu molkg^{-1}$) compared to a linear regression with only SSS ($R^2 = 0.67$; $n = 23$; $\text{RMSE} = 24.0\,\mu molkg^{-1}$). This is probably because SST acts as an indicator of the effect of nutrient cycling on TA in agreement to what has been reported for the open Atlantic Ocean (Lee et al., 2006).

To estimate a corresponding TA value for each UW fCO_2 observation obtained from MS *Trans Carrier*, we used salinity values estimated from the UW SST data by using Eq. (1). The results (denoted as SSS(sst)) were then inputted into Eq. (2) to obtain TA(sst) (see Table 2 for nomenclature). The fact that TA(sst) is based on SSS(sst) rather than measured SSS values introduces an additional error in the estimated pH(sst) and Ω_{Ar}(sst). In order to assess this error we compared pH(sst) and Ω_{Ar}(sst) with values based on the cruise data, i.e. pH(sss) and Ω_{Ar}(sss). First, we computed pH(sss) and Ω_{Ar}(sss) by combining all available measured SSS, estimated TA(sss) from Eq. (2), and co-located UW SST and

Table 2. Overview of the symbols used for quantities estimated and/or derived from the measurement-based variables SSS, SST, TA, pH, DIC, fCO_2, and Ω_{Ar}.

Symbol	Meaning
TA(sss)	TA values estimated from measured SSS and SST using Eq. (2).
pH(sss), Ω_{Ar}(sss)	pH, and Ω_{Ar} values estimated by combining TA (sss) and fCO_2.
SSS(sst)	SSS values estimated from SST using Eq. (1).
TA(sst)	TA values determined from estimated SSS(sst) and SST using Eq. (2).
pH(sst), Ω_{Ar}(sst), DIC(sst)	Values of pH, Ω_{Ar} and DIC that have been obtained by combining TA (sst), fCO_2 and ancillary variables.
$fCO_{2@meanSST}$	fCO_2 at the mean temperature
nDIC	DIC normalized to the mean salinity

Table 3. Results of the comparisons between measurement-based and estimated values for pH, Ω_{Ar}, SST (°C), and SSS. For the first three parameters, the statistics of the linear relationships depicted in Fig. 2b–d are listed. For SSS, monthly averaged data are compared to estimates obtained with Eq. (1) using monthly SST. For SST, the comparison is carried out to verify that measurements from Raunefjord are representative for the whole study area (i.e. UW_SST can be estimated by RF_SST), which is implicitly assumed by the use of Eq. (1). R^2 is the coefficient of determination, and "RMSE" denotes the root-mean-square error. The latter is compared against benchmarks derived from maximum target uncertainties (max. uncertainty) developed by Global Ocean Acidification Observing Network (Sect. 3.1). The p value is the probability of no linear relation between the estimated and measurement-based values.

Compared variables	Comparison statistics			Benchmarks	
	R^2	p value	No. points	RMSE	Max. uncertainty
pH_meas/comp. and pH(sst)	1.00	< 0.001	106	0.003	±0.02
Ω_{Ar}_computed and Ω_{Ar}(sst)	0.98	< 0.001	106	0.04	±0.2
UW_SST and RF_SST	0.95	< 0.001	61	0.49	±1.25
SSS and SSS(sst)	0.65	0.002	12	0.3	±1.8

UW fCO_2. Then we repeated the calculations, but this time we replaced the measured SSS with estimated SSS(sst) from Eq. (1) to compute pH(sst) and Ω_{Ar}(sst). The very strong linear relationships ($R^2 \approx 1$) between the resulting values in Fig. 2c and d (circles) confirm that the estimated pH(sst) and Ω_{Ar}(sst) reproduce closely the measurement-based values of pH(sss) and Ω_{Ar}(sss) for the whole study area. This is also evident from comparison statistics on rows 1 and 2 in Table 3, which show that measured-based values are well correlated ($R^2 \approx 1$, $p < 0.001$) with those estimated with RMSE values of 0.003 and 0.04 for pH(sss) and Ω_{Ar}(sst), respectively, which are well within the aforementioned maximum target uncertainties developed by the C-CAN (last column in Table 3).

To quantify the total error associated with the pH(sst) and Ω_{Ar}(sst) estimates, we considered two main sources for error. First we computed the residuals (estimated – measurement-based) using the data shown in Fig. 2c and d (including the sensor data). The mean difference for the whole study area was 0.002 ± 0.004 and 0.005 ± 0.08 for pH and Ω_{Ar}, respectively. Thus, the maximum probable error from this source is 0.006 and 0.09 for pH and Ω_{Ar}, respectively. Additionally, we estimated that the computed and/or measured pH values included an error of 0.012 pH units, which under the current conditions (mean TA, fCO_2, SST, and SSS) would give an error of 0.09 in Ω_{Ar}. These two error estimates were combined (as the square root of sum of squares) to determine the total error in our estimates, which were found to be ±0.013 and ±0.13 for pH and Ω_{Ar}, respectively. It must be noted that the above total error was derived from all available observational data including the in situ sensor data (shown in Fig. 2c and in described Sect. 2.3), which are the only wintertime measurements used in this study. This is important because the lack of wintertime data in the CS data set that was used for the identification of TA-SSS/SST relationship (Eq. 2), means that wintertime TA(sst) might be overestimated so that corresponding pH(sst) values would be overestimated. In fact, during the aforementioned comparison between pH(sst) and measured pH we noted that for this particular data set pH(sst) overestimated the measurements. However, the estimates were consistent with the observations to within the total error of ±0.01 pH units. Thus, by utilizing the above total errors, we also accounted for the effect of this possible caveat of Eq. (2) arising from the lack of wintertime TA measurements.

From the above we conclude that we are able to estimate pH(sst) and Ω_{Ar}(sst) across the whole study area and during all seasons with total errors of ±0.01 and ±0.1 for pH and Ω_{Ar}, respectively.

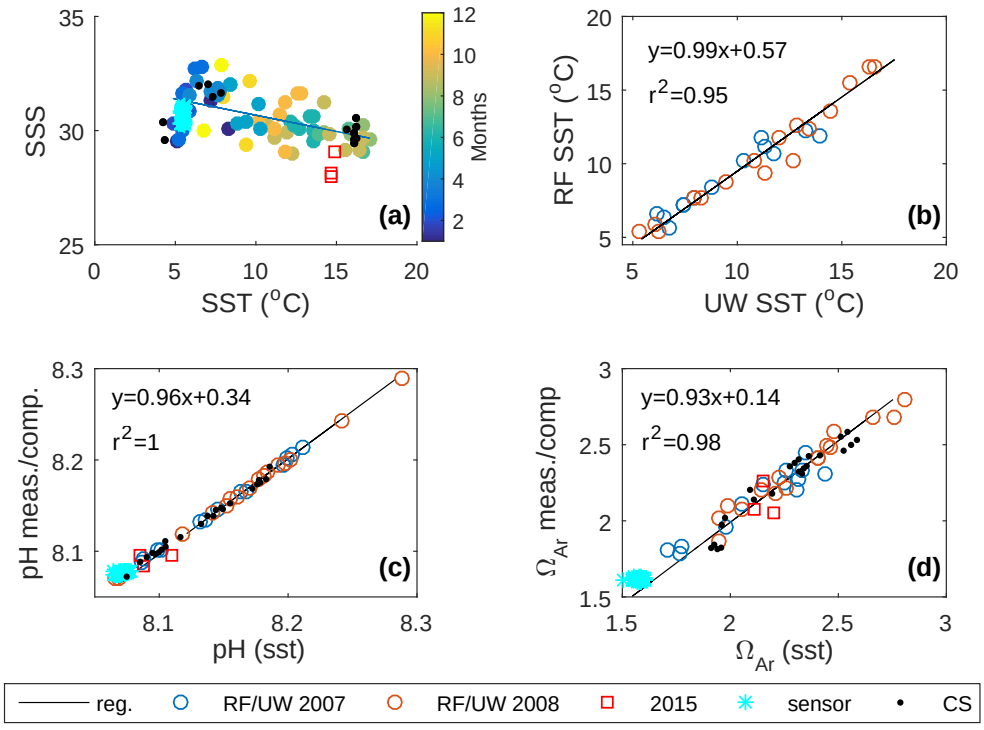

Figure 2. **(a)** RF SSS as a function of SST (filled symbols) with the regression line described by Eq. (1). Sampling month is indicated by the colour of the data points. The CS (dots), 2015 (squares), and sensor (stars) data sets are also shown for comparison with the regression line. **(b)** Compares RF SST with chronologically co-located UW SST acquired from the whole study area during 2008 (blue) and 2007 (red). **(c)** Compares pH(sst) with pH values that have been measured or computed from TA and DIC. Symbols are as in Fig. 1. **(d)** Compares Ω_{Ar}(sst) with Ω_{Ar} values that have been computed from measured TA and DIC or from measured pH and UW fCO_2. Symbols are as in Fig. 1. In the legend, "reg." means regression line.

3.2 Spatiotemporal variations

In order to present the mean distributions across the different fjords throughout the annual cycle, we condensed the data into one virtual year by projecting it onto non-equidistant rectangular grids using the "weighted-average gridding" method of the Ocean Data View software (Schlitzer, 2015). As evident from Fig. 3, there is a clear seasonality (for the interannual changes see Sect. 3.3) in both pH(sst) and Ω_{Ar} (sst). The former varies between minimum values (8.05) around the 1 January to typical maximum values of around 8.25, which occur during the late winter and/or spring (March–April). This increase is due to the reduction of DIC (Fig. 3d), induced by the phytoplankton spring bloom. This clearly counteracts and outweighs the negative effect on pH of warming the water column during this period. However, during April/May, the effect of warming begins to dominate and pH(sst) starts decreasing. By September the SST starts decreasing, while pH continues to drop. This is due to the effect of the fall mixing, which enables carbon-rich coastal water to reach the surface layer, as mentioned in Sect. 1, and is reflected by increasing DIC during this period (Fig. 3d).

The mean distribution of Ω_{Ar}(sst) also shows a significant seasonal variation. There are three factors that drive this: (i) reduced concentrations of DIC by the spring bloom increases the concentration of carbonate ions, (ii) Ω_{Ar}(sst) increases with rising temperature so that warming during the summer actually reinforces the increase of Ω_{Ar} initiated by biological carbon uptake, and (iii) reduced TA due to freshwater input from run-off and mixing of deeper carbon-rich water into surface layer reduce Ω_{Ar}(sst) during fall. Thus, Ω_{Ar}(sst) reaches its maximum (>2.5) in July–September, when the spring bloom is over and pH has already started decreasing (Fig. 3a, c). The lowest Ω_{Ar}(sst) values (≈ 1.3–1.6) occur during winter (January–March) when both pH and SST are low, despite TA being high due to high SSS values. The decoupling in the seasonal cycles of pH and Ω_{Ar} clearly supports the case that pH alone is not an adequate measure of ocean acidification, in accordance with the C-CAN recommendation that "measurements should facilitate determination of Ω_{Ar} and a complete description of the carbonate system, including pH and pCO_2" (McLaughlin et al., 2015).

The above-described seasonal variations in pH(sst) and Ω_{Ar}(sst) are spatially more or less coherent within the whole study area, except for the slight south–north gradient during May–September, with the highest values south of 60°N (see Fig. 3a, c). All in all, during summertime the study area em-

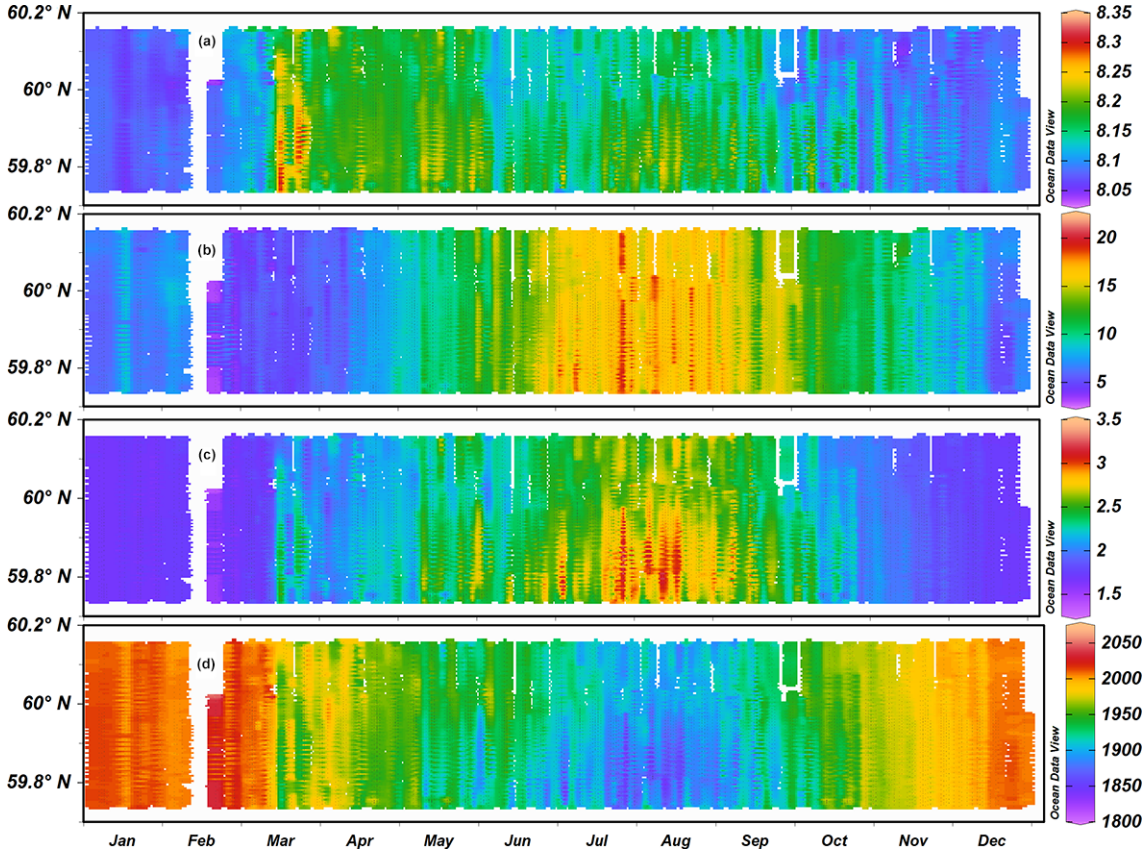

Figure 3. **(a)** Estimated pH(sst), **(b)** UW SST, **(c)** estimated Ω_{Ar}(sst), and **(d)** estimated DIC, which have been normalized to the mean salinity of 30.5 as a function of latitude and time of the year. All data from 2005 to 2009 have been condensed into one virtual year to resolve the spatial and seasonal variations.

bodied warm surface water with high Ω_{Ar}(sst) and intermediate pH(sst) values. During winter, the surface water is cold with low Ω_{Ar}(sst) and pH(sst) values.

3.3 Controls of seasonal variability and trends

To investigate the seasonal variability more thoroughly, we computed monthly averages of pH(sst), SST, Ω_{Ar}(sst), and nDIC(sst) for one composite year. Then we quantified the effect of DIC, TA, SST, and SSS on the monthly changes of pH(sst) and Ω_{Ar}(sst) in order to gain more insight into the processes governing the seasonal variations and their relative importance (Fig. 4).

For pH(sst) we used the decomposition method described in Lauvset et al. (2015) to quantify the importance of different parameters. This method estimates the monthly pH changes expected from corresponding changes observed in SST, SSS, DIC, and TA as well as their sum. The results are shown in Fig. 4a–e where it can be seen that DIC is the most important driver followed by SST and TA, whereas SSS had a negligible effect (not shown) on the seasonal pH variations. We also note that the effects of SST and TA combined are nearly equal to, but opposite of, that of DIC (Fig. 4c, d, e). As a result, the sum of all effects is <0.06 pH units, and compares well to the observed amplitudes (Fig. 4a), meaning that the decomposition model is able to account for the observed seasonal changes. Note also the TA control is identical to that of SST (Fig. 4c, e). The reason for this is that TA values used here are obtained from SSS(sst) and SST using Eq. (2), which in effect means that they are based on SST. This emphasizes the need for measured SSS and TA values when the objective is to analyse the controls of pH and Ω_{Ar}(sst) variations.

For Ω_{Ar}(sst) we investigated the importance of different controls (DIC, TA, SST, SSS) by varying them independently over their observed range, while holding all other drivers constant, and re-computing Ω_{Ar}(sst). The magnitude of the standard deviation of the results is indicative of the importance of the varying drivers. The result of this exercise is shown in Fig. 4f–i. Evidently, the variations of SST and SSS are the least important drivers for Ω_{Ar}(sst) seasonal changes, since varying these parameters induces changes that are about an order of magnitude less than the observed seasonal amplitude in Ω_{Ar}(sst). On the other hand, changing DIC and TA (Fig. 4h, i) induces changes that are comparable to the seasonal amplitude observed in Ω_{Ar}(sst) (Fig. 4a). We

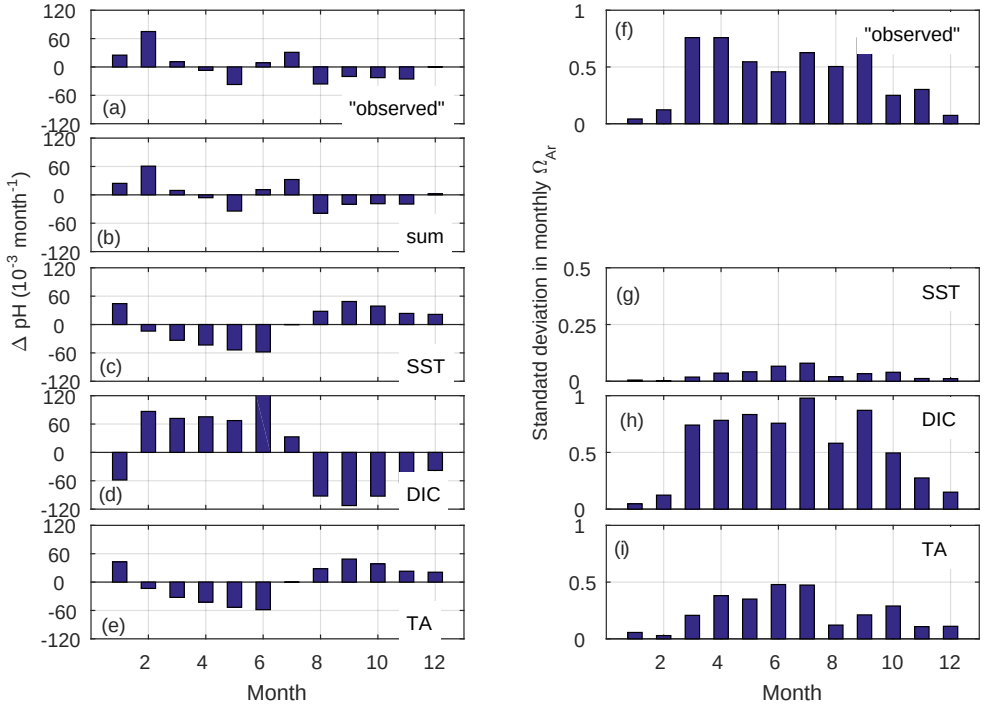

Figure 4. Left panel: monthly pH changes (ΔpH) as observed **(a)** and expected due to sum of all derivers **(b)**, SST changes **(c)**, DIC changes **(d)**, and by TA changes **(e)**. Right panel: standard deviations in monthly mean Ω_{Ar} as a result of variations in all parameters **(f)** or only in SST **(g)** in DIC **(h)** in TA **(i)**.

therefore conclude that seasonal changes in DIC and TA are the most important drivers for changes in Ω_{Ar}(sst).

From the above we conclude that the main drivers of Ω_{Ar}(sst) are DIC and TA, whereas for pH(sst), SST also has a significant impact. This means that the formation and destruction of organic matter together with upwelling of carbon-rich coastal water, seasonal warming and cooling, and run-off inputs, are the processes that govern most of the seasonal variability of OA parameters within the study area. It then follows that interannual variability in the above processes would lead to corresponding variations in pH(sst) and Ω_{Ar}(sst). Such interannual changes are evident from the monthly time series (Fig. S1 in Supplement), where the rate of seasonal change differs between the years, both for SST and DIC normalized to the mean salinity (nDIC) according to Friis et al. (2003). Additionally, for SST, the extreme values also change between the years. These changes are in turn reflected in the pH(sst) and Ω_{Ar}(sst) for which the amplitude of the interannual variability (IAV), calculated as the temporal standard deviation, is presented in Table 4. For pH, IAV was normally much lower than the seasonal changes and ranged between 0.01 and 0.02 although higher changes were observed during the months April (0.04), and July and October (0.03). Similarly, for Ω_{Ar}(sst), the IAV was typically 0.1, which is much lower than the seasonal changes (Sect. 3.2). Higher IAVs were observed for June (0.2) whereas November and December showed the lowest IAVs (< 0.05). Quantitatively, the above IAVs are probably lower limits due to the use of constant empirical relationships for the estimation of SSS and TA (Eqs. 1 and 2). That is, there may be interannual changes in the relationship between SST and SSS (Eq. 1) and/or between SSS/SST and TA (Eq. 2). Thus, the use of a constant relationship over the years may have led to underestimation of the resulting IAV. Consequently, a comprehensive analysis of the drivers of the IAV was not carried out in this study. However, the sensitivity computations we performed showed that year-to-year differences in pH were related to those in fCO_2 rather than SST changes, whereas year-to-year differences in Ω_{Ar}(sst) were more related to those in SST than fCO_2. In any case, the observed year-to-year differences were not systematic, and no multiyear temporal trend was apparent from the 4-year time series analysed in this study.

3.4 Inference of OA parameters from VOS underway data

Changes in the oceanic CO_2-system variables are related through ratios called Buffer Factors. Specifically, changes in Ω_{Ar} and pH in response to aqueous CO_2 ($[CO_2(aq)] = [CO_2] + H_2CO_3$], henceforth denoted as CO_2) variations can be quantified by partial derivatives ($\gamma_{DIC} = (\partial \ln CO_2/\partial DIC)^{-1}$, $\beta_{DIC} = (\partial H^+/\partial DIC)^{-1}$, and $\omega_{DIC} = (\partial \ln \Omega/\partial DIC)^{-1}$), which have been defined by Egleston et

Table 4. Monthly mean values for pH(sst) and Ω_{Ar}(sst) and associated interannual variability (IAV), computed as standard deviations, in the study area for the period 2005–2009.

		Jan	Feb	Mar	Apr	May	Jun	Jul	Aug	Sep	Oct	Nov	Dec
pH(sst)	Mean	8.08	8.10	8.16	8.19	8.18	8.15	8.15	8.17	8.14	8.11	8.10	8.08
	IAV	<0.01	0.01	0.04	0.01	0.02	0.02	0.03	0.02	0.02	0.03	0.02	0.02
Ω_{Ar}(sst)	Mean	1.7	1.7	1.9	2.1	2.3	2.4	2.6	2.7	2.4	2.2	1.9	1.8
	IAV	0.1	0.1	0.1	0.1	0.1	0.2	0.1	0.1	0.1	0.1	<0.05	<0.05

al. (2010, their Table 1), and the slope of these relationships can be expressed mathematically by

$$\partial \ln \Omega / \partial \ln CO_2 = \gamma_{DIC}/\omega_{DIC} = \frac{DIC - Alk_C^2/S}{DIC - Alk_C P/HCO_3^-}, \quad (3)$$

$$\partial \ln H^+ / \partial \ln CO_2 = \gamma_{DIC}/\beta_{DIC} = \frac{(DIC - Alk_C^2)/S}{(DICS - Alk_C^2)/Alk_C}, \quad (4)$$

where expressions for the carbonate alkalinity Alk_C and the parameters P and S are defined in Egleston et al. (2010). We have evaluated the right-hand sides of Eqs. (3) and (4), using the CS cruise data, and the results showed that these quantities change only a few per cent (1.3 and 3.4 %, respectively) due to seasonal changes in the various variables. The ratio $\gamma_{DIC}/\omega_{DIC}$ changed by 1–6 % and ranged from −1.08 to −0.980, while γ_{DIC}/β_{DIC} changed by 0.5–3 % and ranged from 0.84 to 0.88. This, together with the fact that equations 3 and 4 can be defined in terms of $\ln(fCO_2)$ instead of $\ln(CO_2)$ (Egleston et al., 2010; Takahashi et al., 1993), suggests that in situations where underway surface fCO_2 and SST are frequently measured, whereas the CO_2 system is fully determined only occasionally, an easy way of interpolating the seasonality in pH and Ω_{Ar}, is to predict them from fCO_2. We have implemented this alternative way of estimating pH and Ω_{Ar} using the CS cruise data. For the estimation of Ω_{Ar} we used $fCO_{2@meanSST}$, which is fCO_2 adjusted to constant temperature (i.e. at mean SST), because this normalization improved the regression significantly. Since we were interested in pH and Ω_{Ar} we plotted these parameters directly against $\ln(fCO_2)$ or $\ln(fCO_{2t@meanSST})$. The results are shown in Fig. 5 and conform to tight relationships between computed pH and $\ln(fCO_2)$ values (Fig. 5a), and between computed Ω_{Ar} and $\ln(fCO_{2t@meanSST})$ (Fig. 5b). Further, by using linear curve fitting we determined the relationships according to

$$pH = -0.389 \ln fCO_2 + 10.354$$
$$R^2 = 0.99; n = 28; RMSE = 0.005, \quad (5)$$
$$\Omega_{Ar} = \exp(-0.6741 \ln fCO_2 \text{ at mean SST} + 4.6422)$$
$$R^2 = 0.94; n = 28; RMSE = 0.07. \quad (6)$$

The magnitude of the residuals (computed – estimated) associated with pH and Ω_{Ar} values obtained from the above relationships were 0.000 ± 0.005 and 0.01 ± 0.06, respectively, which is comparable to the residuals associated with pH(sst) and Ω_{Ar}(sst) (Table 3). An advantage of this procedure, however, is that it utilizes much tighter empirical relationships, involves fewer computational steps, and is based on UW data, which are much more numerous than station data from oceanography cruises. Thus, it minimizes errors introduced by intermediate results such as the TA-SSS/SST regression in Eq. (2) and/or seasonal data coverage. Furthermore, a direct comparison revealed that values obtained from Eqs. (5) and (6) were almost identical to those of pH(sst) and Ω_{Ar}(sst) (Fig. S2) with values for R^2, p value, and RMSE of 1, 0, and 0.003 for pH; and 1, 0, and 0.02 for Ω_{Ar}. However, it is important to realize that for the above procedure too, a representative full description of the carbonate system is necessary for up-to-date determinations of Eqs. 5 and 6. Further, this calibration data ideally should include high-frequency time series observations, since the slopes (i.e. Eqs. 3 and 4) change slightly with the carbonate system variables (e.g. DIC and TA; see Eqs. 3 and 4), which vary on multiple timescales (hours–days–years). Furthermore, the procedure is based on measurements of only one of the four master parameters constituting the carbonate system (i.e. fCO_2). Therefore, it only provides a way to interpolate pH and Ω_{Ar} values, but cannot support the analyses of controls that have been provided in the proceeding section.

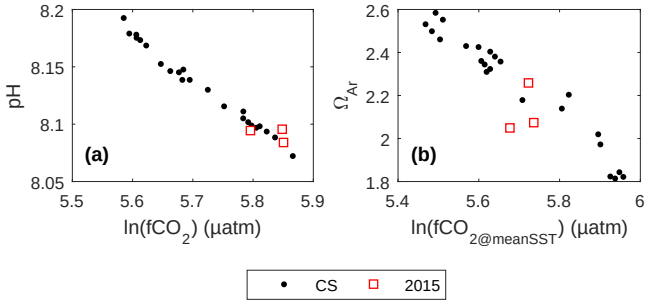

Figure 5. **(a)** and **(b)** pH and Ω_{Ar} from CS (dots) and 2015 (red squares) cruises plotted as a function of $\ln(fCO_2)$ and $\ln(fCO_{2\,meanSST})$, respectively.

From Fig. 5b we note that lowest Ω_{Ar} values are associated with the highest $fCO_{2@meanSST}$ values, which occur during late fall and winter. Monitoring of these extreme val-

ues are of special interest because (i) during late fall and early winter the upwelling of carbon-rich water occurs and surface water also reflects the properties of the deeper water, and (ii) the rate of change at this point (lowest Ω_{Ar}, highest $fCO_{2@meanSST}$) indicates the time when under-saturation of calcium carbonate can be expected in these waters. To estimate this for the current data we used Eq. 5 and the observation that the slope (i.e. Eq. 3) and intercept decreased by about 0.0008 and 0.004 for every 1 µatm increase in mean $fCO_{2@meanSST}$. We also took into account an uncertainty of ± 0.2 in the Ω_{Ar} estimates and found that Ω_{Ar} becomes undersaturated (< 1) when mean annual $fCO_{2@meanSST}$ is about 310 ± 70 µatm higher than its present value (310 µatm). For business as usual emission scenario (RCP 8.5), this is equivalent to about year 2070 ± 10 if we assume that the development in the ocean follows that of the atmosphere (i.e. constant disequilibrium between ocean and atmosphere).

4 Summary and conclusions

We have been able to determine, for the first time, the seasonal changes and drivers of pH and ΩAr across western Norwegian fjords (59.74–60.23°N and 5.16–5.6°E), based on underway fCO_2 and SST data combined with sporadic data from research cruises and empirical relationships.

During summertime the study area embodied warm surface water with high ΩAr (< 2.5) and intermediate pH values (8.12–8.17). During winter, the surface water was cold with low ΩAr and pH values, 1.3–1.6 and 8.05–8.07, respectively. Maximum pH of 8.25 was encountered during the phytoplankton spring bloom (March–April). Seasonal changes in DIC, TA, and SST were the most important drivers of pH and ΩAr changes, although the SST influence on ΩAr was only weak.

Measurement errors together with seasonal and spatial gaps in the data used to identify the empirical relationships are considered as two main sources for uncertainties, and the computed total errors associated with the estimated values (± 0.01 and ± 0.1 for pH and ΩAr) are about 50 % of the maximum target uncertainties developed by the Global Ocean Acidification Network.

We have shown that the strong correlations of pH and ΩAr with fCO_2 and $fCO_{2@meanSST}$ (fCO_2 adjusted to the mean temperature), respectively, provide an approach to interpolate pH and ΩAr values both seasonally and spatially. Furthermore, the ΩAr–$fCO_{2@meanSST}$ relationship, as well as the rate of change of its slope and intercept with DIC, has been used to estimate that under-saturation of the aragonite mineral can occur in the study area by the year 2070 ± 10, if we assume a business as usual emission scenario (RCP 8.5) and constant CO_2 disequilibrium between ocean and atmosphere.

The Supplement related to this article is available online at doi:10.5194/os-12-937-2016-supplement.

Acknowledgements. We are grateful for financial support by the Research Council of Norway (RCN) through the project FME SUCCESS, and by the Norwegian Environment Agency through the project *Havforsuring*. The data collection has been financed by the EU IP CARBOOCEAN (contract no. 511176-2). This work would not have been possible without the generosity and help of the liner company SeaTrans AS and the captains and crew of MS *Trans Carrier*. We are grateful for the technical assistance provided by Tor de Lange, Kristin Jackson, and Tomas Sørlie, and for encouraging and constructive comments from the reviewers (Dr. M. Riba-Ribas and Dr. E. M. Jones) and the topic editor Dr. Mario Hoppema that have improved the manuscript.

Edited by: M. Hoppema
Reviewed by: E. M. Jones and M. Ribas-Ribas

References

Asplin, L., Johnsen, I. A., Sandvik, A. D., Albretsen, J., Sundfjord, V., Aure, J., and Boxaspen, K. K.: Dispersion of salmon lice in the Hardangerfjord, Mar. Biol. Res., 10, 216–225, 2014.

Aure, J. and Stigebrandt, A.: On the influence of topographic factors upon the oxygen consumption rate in sill basins of fjords, Estuar. Coast. Shelf Sci., 28, 59–69, 1989.

Bach, L. T.: Reconsidering the role of carbonate ion concentration in calcification by marine organisms, Biogeosciences, 12, 4939–4951, doi:10.5194/bg-12-4939-2015, 2015.

Bakke, J. L. W. and Sands, N. J.: Hydrographical studies of Korsfjorden, western Norway, in the period 1972–1977, Sarsia, 63, 7–16, 1977.

Bakker, D. C. E., Pfeil, B., Smith, K., Hankin, S., Olsen, A., Alin, S. R., Cosca, C., Harasawa, S., Kozyr, A., Nojiri, Y., O'Brien, K. M., Schuster, U., Telszewski, M., Tilbrook, B., Wada, C., Akl, J., Barbero, L., Bates, N. R., Boutin, J., Bozec, Y., Cai, W. J., Castle, R. D., Chavez, F. P., Chen, L., Chierici, M., Currie, K., de Baar, H. J. W., Evans, W., Feely, R. A., Fransson, A., Gao, Z., Hales, B., Hardman-Mountford, N. J., Hoppema, M., Huang, W. J., Hunt, C. W., Huss, B., Ichikawa, T., Johannessen, T., Jones, E. M., Jones, S. D., Jutterström, S., Kitidis, V., Körtzinger, A., Landschützer, P., Lauvset, S. K., Lefèvre, N., Manke, A. B., Mathis, J. T., Merlivat, L., Metzl, N., Murata, A., Newberger, T., Omar, A. M., Ono, T., Park, G. H., Paterson, K., Pierrot, D., Ríos, A. F., Sabine, C. L., Saito, S., Salisbury, J., Sarma, V. V. S. S., Schlitzer, R., Sieger, R., Skjelvan, I., Steinhoff, T., Sullivan, K. F., Sun, H., Sutton, A. J., Suzuki, T., Sweeney, C., Takahashi, T., Tjiputra, J., Tsurushima, N., van Heuven, S. M. A. C., Vandemark, D., Vlahos, P., Wallace, D. W. R., Wanninkhof, R., and Watson, A. J.: An update to the Surface Ocean CO_2 Atlas (SOCAT version 2), Earth Syst. Sci. Data, 6, 69–90, doi:10.5194/essd-6-69-2014, 2014.

Bates N. R., Asto, Y., Church, M., Currie, K., Dore, J., González-Dávila, M., Lorenzoni, L., Muller-Karger, F., Olafsson, J., and

Santana-Casiano, J.: A time-series view of changing ocean chemistry due to ocean uptake of anthropogenic CO_2 and ocean acidification, Oceanography, 27, 126–141, 2014.

Bellerby, R. G. J., Olsen, A., Furevik, T., and Anderson, L. A.: Response of the surface ocean CO_2 system in the North Atlantic to climate change, in: The Nordic Seas: An integrated perspective, edited by: Drange, H., Dokken, T. M., Furevik, T., Gerdes, R., and Berger, W. Geophysical Monograph Series, AGU, 2005.

Berge, G.: Discoloration of the sea due to Coccolithus huxleyi bloom, Sarsia, 6, 27–40, 1962.

Borges, A. V.: Do we have enough pieces of the jigsaw to integrate CO_2 fluxes in the coastal ocean?, Estuaries, 28, 3–27, 2005.

Bozec, Y., Thomas, H., Elkalay, K., and de Baar, H. J. W.: The continental shelf pump for CO_2 in the North Sea – evidence from summer observations, Mar. Chem., 93, 131–147, 2005.

Bozec, Y., Thomas, H., Schiettecatte, L.-S., Borges, A.V., Elkalay, K., and de Baar, H. J. W.: Assessment of the processes controlling the seasonal variations of dissolved inorganic carbon in the North Sea, Limnol. Oceanogr., 51, 2746–2762, 2006.

Brattegard, T., Høisæter, T., Sjøtun, K., Fenchel, T., and Uiblein, F.: Norwegian fjords: From natural history to ecosystem ecology and beyond, Mar. Biol. Res., 7, 421–424, 2011.

Cai, W.-J., Dai, M., and Wang, Y.: Air-sea exchange of carbon dioxide in ocean margins: a province-based synthesis, Geophys. Res. Lett., 33, L12603, doi:10.1029/2006GL026219, 2006.

Chavez, F. P., Takahashi, T., Cai, W. J., Friederich, G., Hales, B., Wanninkhof, R., and Feely, R. A.: Coastal Oceans, in: The First State of the Carbon Cycle Report (SOCCR), edited by: King, A. W., Dilling, L., Zimmerman, G. P., Fairman, D. M., Houghton, R. A., Marland, G. H., Rose, A. Z., and Wilbanks, T. J., NOAA, Natl. Clim. Data Cent., Asheville, N.C., 149–156, 2007.

Chen, C.-T. A. and Borges, A. V.: Reconciling opposing views on carbon cycling in the coastal ocean: continental shelves as sinks and near-shore ecosystems as sources of atmospheric CO_2, Deep-Sea Res. Pt. II, 56, 578–90, 2009.

Ciais, P., Sabine, C., Bala, G., Bopp, L., Brovkin, V., Canadell, J., Chhabra, A., DeFries, R., Galloway, J., Heimann, M., Jones, C., Le Quéré, C., Myneni, R. B., Piao, S., and Thornton, P.: Carbon and Other Biogeochemical Cycles, in: Climate Change: The Physical Science Basis, Contribution of Working Group I to the Fifth Assessment Report of the Intergovernmental Panel on Climate Change, edited by: Stocker, T. F., Qin, D., Plattner, G.-K., Tignor, M., Allen, S. K., Boschung, J., Nauels, A., Xia, Y., Bex, V., and Midgley, P. M.: Cambridge University Press, Cambridge, United Kingdom and New York, NY, USA, 465–570, doi:10.1017/CBO9781107415324.015, 2013.

Clargo, N. M., Salt, L. A., Thomas, H., and de Baar, H. J. W.: Rapid increase of observed DIC and pCO_2 in the surface waters of the North Sea in the 2001–2011 decade ascribed to climate change superimposed by biological processes, Mar. Chem., 177, 566–581, 2015.

Egleston, E. S., Sabine, C. L., and Morel, F. M. M.: Revelle revisited: Buffer factors that quantify the response of ocean chemistry to changes in DIC and alkalinity, Global Biogeochem. Cycl., 24, GB1002, doi:10.1029/2008GB003407, 2010.

Erga, S. R.: Ecological studies on the phytoplankton of Boknafjorden, western Norway, I. The effect of water exchange processes and environmental factors on temporal and vertical variability of biomass, Sarsia, 74, 161–176, 1989.

Erga, S. R. and Heimdal, B. R.: Ecological studies on the phytoplankton of Korsfjorden, western Norway. The dynamics of a spring bloom seen in relation to hydrographical conditions and light regime, J. Plankt. Res., 6, 67–90, 1984.

Fosså, J. H., Mortensen, P. B., and Furevik, D. M.: The deep-water coral Lophelia pertusa in Norwegian waters: distribution and fishery impacts, Hydrobiologia, 471, 1–12, 2002.

Fransson, A., Chierici M., Nomura, D., Granskog, M. A., Kristiansen, S., Martma, T., and Nehrke, G.: Effect of glacial drainage water on the CO_2 system and ocean acidification state in an Arctic tidewater-glacier fjord during two contrasting years, J. Geophys. Res.-Ocean., 120, 2413–2429, 2015.

Frette, Ø., Erga, S. R., Hamre, B., Aure, J., and Stamnes, J. J.: Seasonal variability in inherent optical properties in a western Norwegian fjord, Sarsia, 89, 276–291, 2004.

Friis, K., Kortzinger, A., and Wallace, D. W. R.: Salinity normalization of marine inorganic carbon chemistry data, Geophys. Res. Lett., 30, 1085, doi:10.1029/2002GL015898, 2003.

Gattuso, J.-P. and Hansson, L. (Eds.): Ocean Acidification, Oxford Univ. Press, Oxford, UK, 2011.

Helle, H. B.: Summer replacement of deep water in Byfjord, western Norway: mass exchange acros the sill induced by upwelling, in: Hydrodynamics of estuaries and fjords proceedings of the 9th Liege Colloquium on Ocean Hydrodeynamics, edited by: Nihoul, J. C. J., Elsevier, 441–464, 1978.

Johannessen, A., Skaret, G., Langård, L., Slotte, A., Husebø, Å., and Fernö, A.: The dynamics of a metapopulation: Changes in life-history traits in resident herring that co-occur with oceanic herring during spawning, PLoS ONE, 9, e102462, doi:10.1371/journal.pone.0102462, 2014.

Johnson, K. M., Wills, K. D., Butler, D. B., Johnson, W. K., and Wong, C. S.: Coulometric total carbon dioxide analysis for marine studies: maximizing the performance of an automated gas extraction system and coulometric detector, Mar. Chem., 44, 167–187, 1993.

Lauvset, S. K., Gruber, N., Landschützer, P., Olsen, A., and Tjiputra, J.: Trends and drivers in global surface ocean pH over the past 3 decades, Biogeosciences, 12, 1285–1298, doi:10.5194/bg-12-1285-2015, 2015.

Lee, K., Tong, L. T., Millero, F. J., Sabine, C. L., Dickson, A. G., Goyet, C., Park, G.-H., Wanninkhof, R., Feely, R. A., and Key, R. M.: Global relationships of total alkalinity with salinity and temperature in surface waters of the world's oceans, Geophys. Res. Lett., 33, L19605, doi:10.1029/2006gl027207, 2006.

Le Quéré, C., Moriarty, R., Andrew, R. M., Canadell, J. G., Sitch, S., Korsbakken, J. I., Friedlingstein, P., Peters, G. P., Andres, R. J., Boden, T. A., Houghton, R. A., House, J. I., Keeling, R. F., Tans, P., Arneth, A., Bakker, D. C. E., Barbero, L., Bopp, L., Chang, J., Chevallier, F., Chini, L. P., Ciais, P., Fader, M., Feely, R. A., Gkritzalis, T., Harris, I., Hauck, J., Ilyina, T., Jain, A. K., Kato, E., Kitidis, V., Klein Goldewijk, K., Koven, C., Landschützer, P., Lauvset, S. K., Lefèvre, N., Lenton, A., Lima, I. D., Metzl, N., Millero, F., Munro, D. R., Murata, A., Nabel, J. E. M. S., Nakaoka, S., Nojiri, Y., O'Brien, K., Olsen, A., Ono, T., Pérez, F. F., Pfeil, B., Pierrot, D., Poulter, B., Rehder, G., Rödenbeck, C., Saito, S., Schuster, U., Schwinger, J., Séférian, R., Steinhoff, T., Stocker, B. D., Sutton, A. J., Takahashi, T., Tilbrook, B., van der Laan-Luijkx, I. T., van der Werf, G. R., van Heuven, S., Vandemark, D., Viovy, N., Wiltshire, A., Zaehle, S., and Zeng, N.:

Global Carbon Budget 2015, Earth Syst. Sci. Data, 7, 349–396, doi:10.5194/essd-7-349-2015, 2015.

Lewis, E. and Wallace, D. W. R.: Program developed for CO_2 system calculations, ORNL/CDIAC-105, Carbon Dioxide Information Analysis Center, Oak Ridge National Laboratory, US Department of Energy, 1998.

Lie, U., Bjørstad, D., and Oug, E.: Eggs and larvae of fish from Lindåspollene, Sarsia, 63, 163–167, 1978.

Lueker, T. J., Dickson, A. G., and Keeling, C. D.: Ocean pCO_2 calculated from dissolved inorganic carbon, alkalinity, and equations for K1 and K2:Validation based on laboratory measurements of CO_2 in gas and seawater at equilibrium, Mar. Chem., 70, 105–119, 2000.

Matthews, J. B. L. and Sands, N.: Ecological studies on the deep-water pelagic community of Korsfjorden, western Norway, The topography of the area and its hydrography in 1968–1972, with a summary of the sampling programmes', Sarsia, 52, 29–52, 1973.

McLaughlin, K., Weisberg, S. B., Dickson, A. G., Hofmann, G. E., Newton, J. A., Aseltine-Neilson, D., Barton, A., Cudd, S., Feely, R. A., Jefferds, I. W., Jewett, E. B., King, T., Langdon, C. J., McAfee, S., Pleschner-Steele, D., and Steele, B.: Core principles of the California Current Acidification Network: Linking chemistry, physics, and ecological effects, Oceanography, 28, 160–169, 2015.

Nondal, G., Bellerby, R. G. J., Olsen, A., Johannessen, T., and Olafsson, J.: Optimal evaluation of the surface ocean CO_2 system in the northern North Atlantic using data from voluntary observing ships, Limnol. Oceanogr. Methods, 7, 109–118, 2009.

Omar, A., Johannessen, T., Bellerby, R. G. J., Olsen, A., Anderson, L. G., and Kivime, C.: Sea-Ice brine formation in Storfjorden: Implications for the Arctic wintertime air – sea CO_2 flux, in: The Nordic Seas: An integrated perspective, Geophysical Monograph Series 158 American Geophysical Union, 177–187, 2005.

Omar, A. M., Olsen, A., Johannessen, T., Hoppema, M., Thomas, H., and Borges, A. V.: Spatiotemporal variations of fCO_2 in the North Sea, Ocean Sci., 6, 77–89, doi:10.5194/os-6-77-2010, 2010.

Provoost, P., van Heuven, S., Soetaert, K., Laane, R. W. P. M., and Middelburg, J. J.: Seasonal and long-term changes in pH in the Dutch coastal zone, Biogeosciences, 7, 3869–3878, doi:10.5194/bg-7-3869-2010, 2010.

Royal Society: Ocean acidification due to increasing atmospheric carbon dioxide, The Royal Society Policy Document 12/05, London, 68 pp., 2005.

Salvanes, A. G. V. and Noreide, J. T.: Dominating sublittoral fish species in a west Norwegian fjord and their trophic links to cod (*Gadus morhua* L.), Sarsia, 78, 221–234, 1993.

Schlitzer, R.: Ocean Data View, https://odv.awi.de/, 2015.

Skagseth, Ø., Drinkwater, K. F., and Terrile, E.: Wind – and buoyancy – induced transport of the Norwegian Coastal Current in the Barents Sea, J. Geophys. Res., 116, doi:10.1029/2011JC006996, 2011.

Stigebrandt, A.: Hydrodynamics and Circulation of Fjords, Encyclopedia of Lakes and Reservoirs, Part of the series Encyclopedia of Earth Sciences Series, 327–344, 2012.

Svendsen, H.: Wind-induced variations of circulation and water level in coupled fjord-coast systems, in: Proc. Symp. Nonv. Coastal Current, Geilo, edited by: Saetre, R. and Mork, M., September 1980, University of Bergen, 229–262, 1981.

Takahashi, T., Olafsson, J., Goddard, J. G., Chipman, D. W. and Sutherland, S. C.: Seasonal variation of CO_2 and nutrients in the high-latitude surface oceans: a comparative study, Global Biogeochem. Cy., 7, 843–878, 1993.

Thomas, H., Bozec, Y., Elkalay, K., and De Baar, H.: Enhanced open ocean storage of CO_2 from shelf sea pumping, Science, 304, 1005–1008, 2004.

Thomas, H., Bozec, Y., Elkalay, K., de Baar, H. J. W., Borges, A. V., and Schiettecatte, L.-S.: Controls of the surface water partial pressure of CO_2 in the North Sea, Biogeosciences, 2, 323–334, doi:10.5194/bg-2-323-2005, 2005.

Thomas, H., Prowe, A. E. F, Van Heuven, S., Bozec, Y., De Baar, H. J. W, Schiettecatte, L.-S., Suykens, K., Koné, M., Borges, A.V., Lima, I. D., and Doney, S. C.: Rapid decline of the CO_2 buffering capacity in the North Sea and implications for the North Atlantic Ocean, Global Biogechem. Cy., 21, GB4001, doi:10.1029/2006GB002825, 2007.

Thomas, H., Schiettecatte, L.-S., Suykens, K., Koné, Y. J. M., Shadwick, E. H., Prowe, A. E. F., Bozec, Y., de Baar, H. J. W., and Borges, A. V.: Enhanced ocean carbon storage from anaerobic alkalinity generation in coastal sediments, Biogeosciences, 6, 267–274, doi:10.5194/bg-6-267-2009, 2009.

van Heuven, S., Pierrot, D., Rae, J. W. B., Lewis, E., and Wallace, D. W. R.: MATLAB Program Developed for CO_2 System Calculations, ORNL/CDIAC-105b, CDIAC, Oak Ridge National Laboratory, Department of Energy, Oak Ridge, Tennessee, USA, doi:10.3334/CDIAC/otg.CO2SYS_MATLAB_v1.1, 2011.

Wootton, J. T., Pfister, C. A., and Forester, J. D: Dynamic patterns and ecological impacts of declining ocean pH in a high-resolution multi-year dataset, PNAS, 105, 18848–18853, 2008.